Geophysical Research Letters

Supporting Information for

Depth-dependent crustal stress rotation and strength variation in the Charlevoix Seismic Zone (CSZ), Québec, Canada

A. Verdecchia[1], J. Onwuemeka[2], Y. Liu[2], and R. M. Harrington[1]

[1]Institute of Geology, Mineralogy and Geophysics, Ruhr-University Bochum, Bochum, Germany.

[2]Department of Earth and Planetary Sciences, McGill University, Montreal, Québec, Canada.

Contents of this file

Introduction

Here we provide a detailed methods description of the moment tensor inversion (Text S1), and additional details about the focal mechanism stress inversion (Text S2), and the coseismic stress changes modeling (Text S3) of the 1663 M 7.5 Charlevoix earthquake. Figure S1 shows a graphical representation of the *b*-values calculated for the entire relocated catalog and for groups of events inside and outside the impact structure. Figure S2 shows the new focal mechanism solutions used in this work in relation to pre-existing solutions from Mazzotti and Townend (2010). Figure S3 shows *b*-values for the entire relocated catalog calculated using magnitudes converted to M_w. Figure S4 supports the hypothesis that a previous large (M 7.5) earthquake in the CSZ has negligible effect on the current regional stress field. Finally, Figures S5 to S10 support the detailed description of the moment tensor inversion methodology from Text S1.

Text S1. Moment tensor inversion

The determination of fault plane solutions is particularly challenging in our study due to poor station coverage (see Figure S5). Although we use waveform data recorded by 11 seismic stations in the CSZ, most of the reported earthquakes are < M 3 with first arrivals exhibiting decreasing impulsive character with increasing source-to-station distance and decreasing event magnitude. The low (<6) number of impulsive first arrival pulses. especially for the smaller (<M

2.5) events, hinders the use of first-motion polarity to infer fault plane solutions. Hence, a full waveform modeling approach is preferred for computing full moment tensor solutions especially for events that do not have impulse first arrivals at available recording stations. We therefore use a probilistic, full waveform modeling algorithm, *Grond*, to invert full moment tensor solutions of 161 earthquakes (Heimann et al., 2018). *Grond* uses an amalgamation of time domain full waveform and cross-correlation, frequency domain amplitude spectra, and time domain envelopes in a Bayesian bootstrap-based probabilistic joint (centroid and moment tensor) inversion technique for source model optimization and uncertainty estimation. The overall uncertainty reflects misfits from each input data form. The joint inversion allows for time shifts to compensate for uncertainty in input velocity model. To avoid distortions due to, for example, incorrect transfer function and low signal-to-noise ratio (SNR), the bootstrap-based optimization performs user-defined independent, parallel runs to generate the final moment tensor solution. *Grond*'s attributes makes it efficient for moment tensor inversion of small earthquakes recorded by sparse surface station networks with low SNR. We refer the reader to Heimann et al. (2018) for additional technical details.

Grond rapidly simulates earthquake waveforms for arbitrary source models from pre-computed Green's Function (GF) databases. We calculate the GF database with QSEIS (Wang, 1999) at a sampling rate of 20 Hz for surface receivers at epicentral distances and depths ranging from 0 - 150 km and 0.5 - 35 km, respectively, with spatial grid spacing of 0.1 km. The GF-database used here is managed by *Fomotso*, and can be downloaded from the Green's Mill web service at https://greens-mill.pyrocko.org/csz 20hz-855580 (last access: June 22, 2022). The 20 Hz sampling rate enables simulation of earthquake waveforms of up to 10 Hz (Nyquist), which is sufficient for moment tensor solutions of the magnitude range observed in this study. The optimum centroid moment tensor solution for each earthquake is determined as the solution with the lowest RMS from a suite of at least 40,000 trials. Each trial solution is results from the fitting of P and S waves in time and spectral domains.

Figure S6 shows focal mechanism solutions for 161 events, where each solution incorporates data from a minimum of 5, 3-component stations. The FMS of the largest event (06/03/2005 MN 4.6) located NE of the impact structure with depth of ~12 km suggests reverse fault motion on a NE-SW trending fault. A comparison of 4 MN > 3 event solutions reported by the Saint Louis University Earthquake Center (SLUEC) moment tensor catalog (SLUEC, 2018) shows similarity between solutions (Figure S7). The rotation angle between two double-couple focal mechanism solutions (Kagan angles) between our solutions and the SLUEC is < 15° (Figure S8), suggesting stable results. We perform an additional consistency check by calculating FMS of 25 events with impulsive first motions at more than 6 stations using *hybridMT* (Kwiatek et al., 2016) and also find consistent results (Figure S9). The Kagan angle of rotation of 84% of the focal mechanism solutions determined by *Grond* and *hybridMT* is less than 35° (Figure S10).

Text S2. Stress inversion

We use the *STRESSINVERSE* package implemented by Vavryčuk (2014) to invert for the principal stress directions. *STRESSINVERSE* applies an iterative procedure to select the nodal plane that is optimally oriented for failure in the estimated stress filed. The algorithm calculates the stress field orientation and the stress ratio in each iteration and selects the nodal plane with the large instability coefficient *I* for the next iteration. *I* is defined as:

$$I = \frac{\tau - \mu(\sigma - 1)}{\mu + \sqrt{1 + \mu^2}},$$

where μ is the apparent coefficient of friction. The variables τ and σ are scaled shear and normal stresses, respectively.

We set $N_{noise\text{-}relatizations} = 500$, $N_{noise\text{-}itarations} = 20$, $N_{relatizations} = 10$, $mean_{deviation} = 20$ (see the associated User Guide available at https://www.ig.cas.cz/en/stress-inverse/). The mean inverted event depth is then used for depth information and for estimating the 95% confidence intervals for the inverted parameters from the 500 noise-realizations.

Text S3. Coseismic stress changes modeling of the 1663 M 7.5 Charlevoix earthquake

Following results from Ebel (2011), we use the software Coulomb 3.4 (Toda et al., 2011) to model a M 7.5 earthquake occurring on a 70 km-long and 15 km-wide thrust fault dipping to the south-east (Figure S4a). We used a heterogeneous slip distribution with a maximum slip of ~11 m located at the center of the fault at ~11 km depth. The resulting static stress drop is 21 MPa, in agreement with the stress drop values calculated for the CSZ (Onwuemeka et al., 2018).

References not included in the manuscript

Kwiatek, G., Martínez-Garzón, P., & Bohnhoff, M. (2016). Hybridmt: A matlab/shell environment package for seismic moment tensor inversion and refinement. *Seismological Research Letters*, 87 (4), 964-976.

Wang, R. (1999). A simple orthonormalization method for stable and efficient computation of green's functions. *Bulletin of the Seismological Society of America*, 89 (3), 733-741.

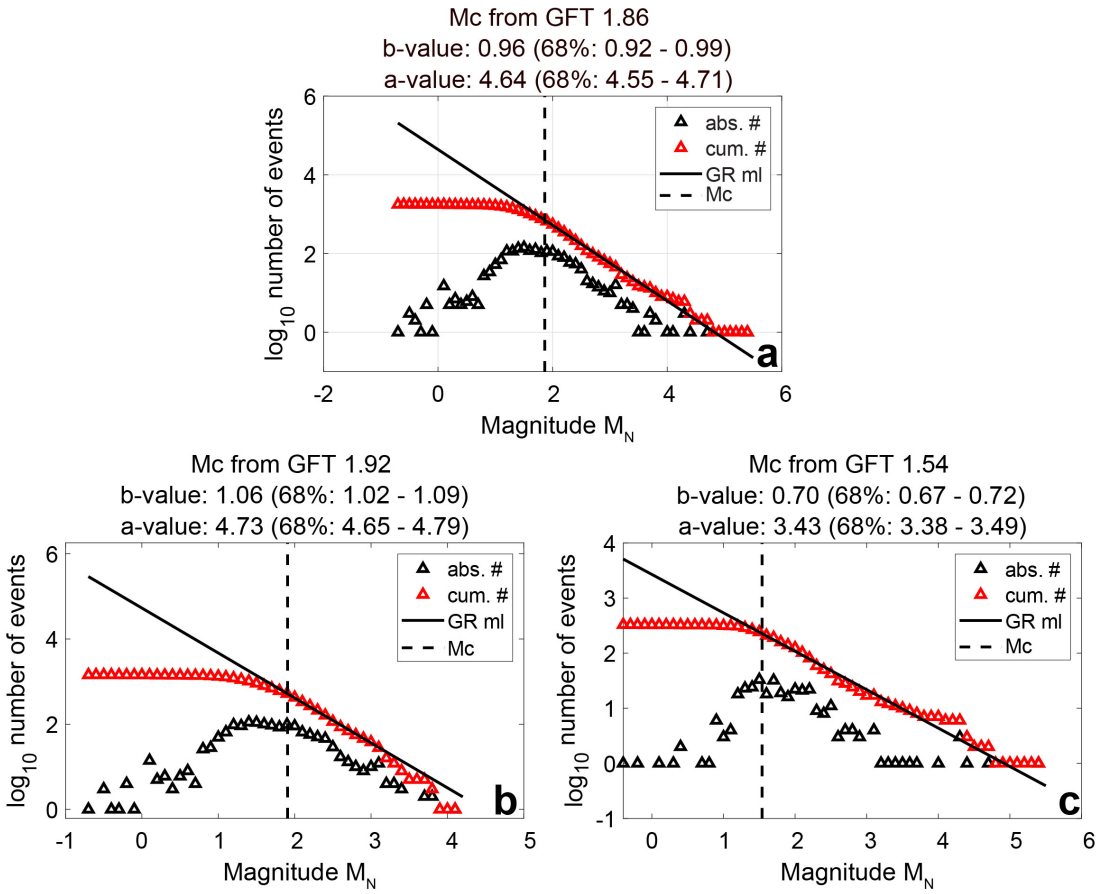

Figure S1. Frequency-magnitude distribution plots for the (a) entire relocated catalog, (b) earthquakes inside the impact structure, and (c) earthquakes outside the impact structure. The solid black lines represent the Gutenberg-Richet fit calculated using the maximum likelihood method (GR ml), while the vertical dashed lines represent the Mc values calculated using the Goodness-of-Fit test (GFT).

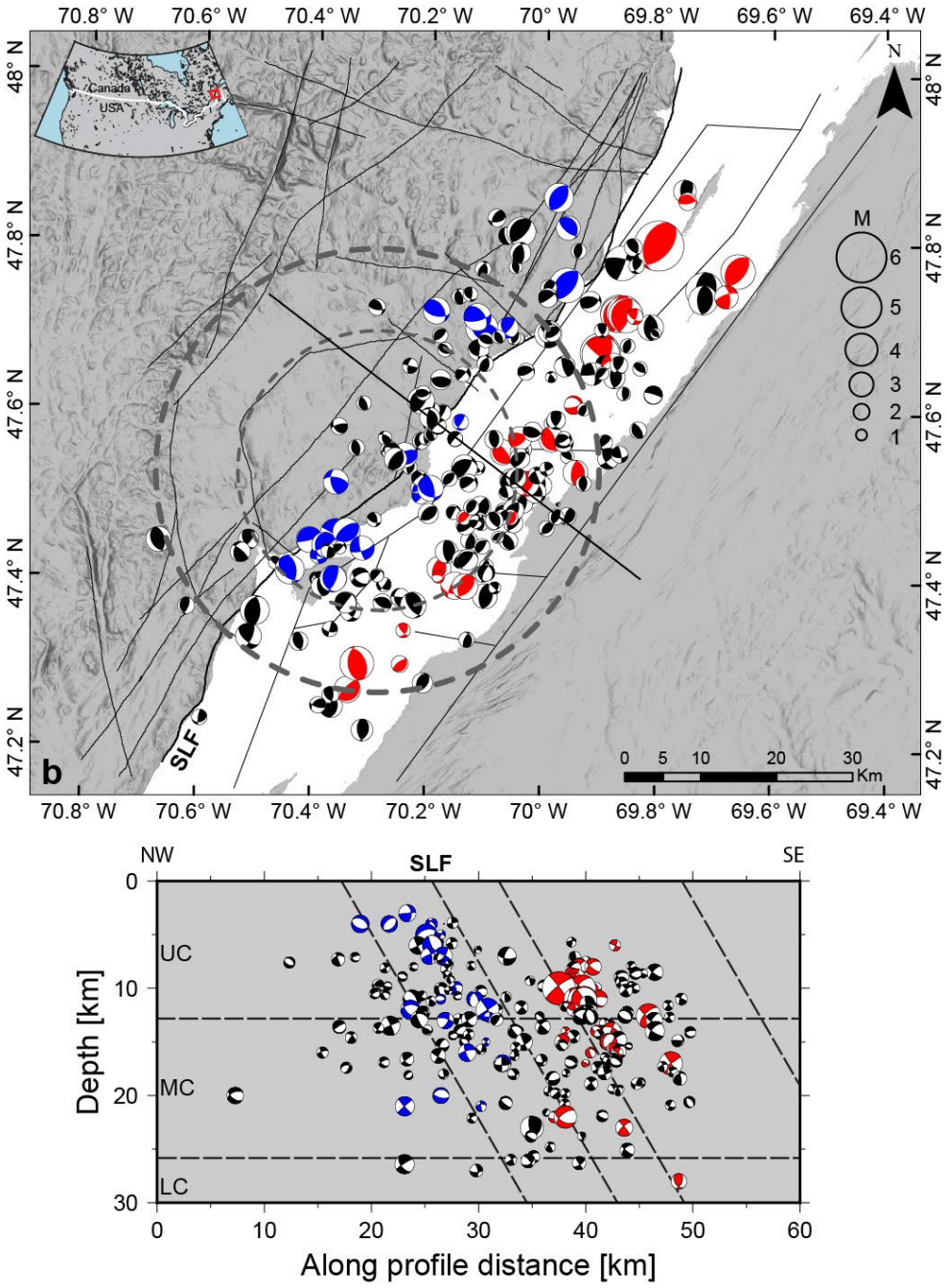

Figure S2. Map and relative cross-section of focal mechanism solutions used in this study. Blue and red FM solutions represent data from Mazzotti and Townend (2010), where blue FMs represent FMs northwest of the Saint-Laurent fault (SLF), and red FMs represent the FMs southeast of the SLF.

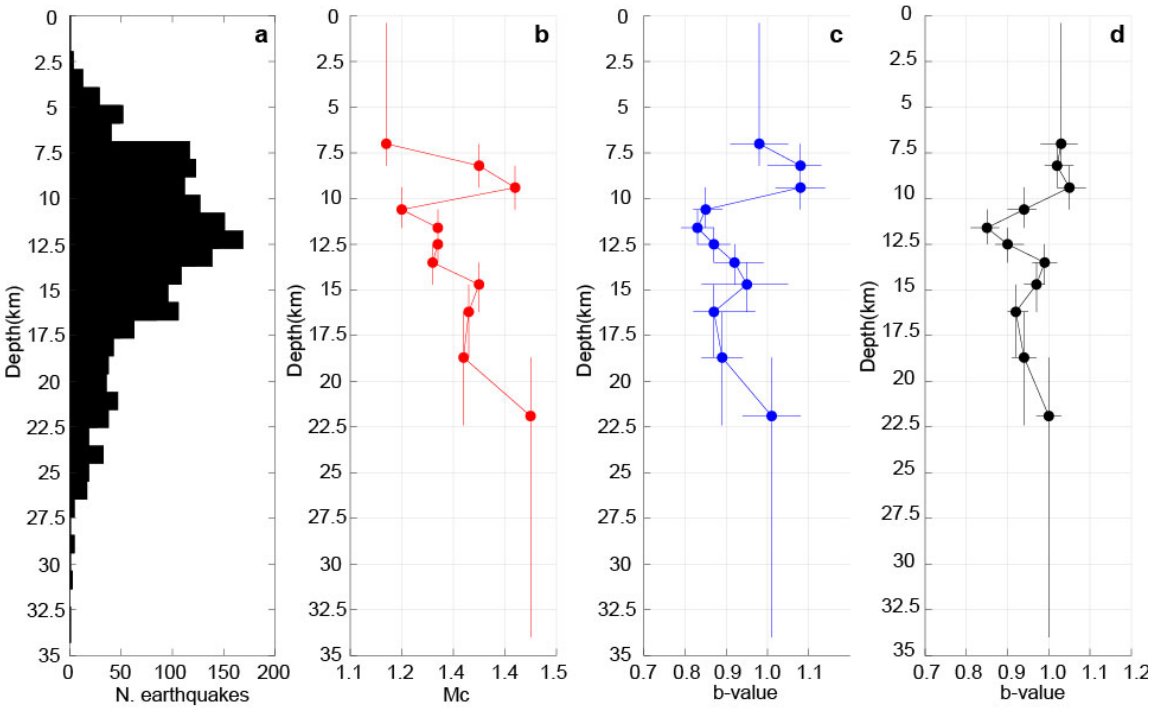

Figure S3. Magnitude-frequency distribution of relocated earthquakes in the CSZ using the catalog converted to M_W. (a) Distribution of earthquakes with depth. (b) Depth-dependent variation of magnitude of completeness (*Mc*) calculated using moving windows of 300 events with 150-event overlap. (c) Depth-dependent *b*-value variation calculated using *Mc* in (b). (d) Depth-dependent *b*-value variation calculated using a fixed *Mc* = 1.45.

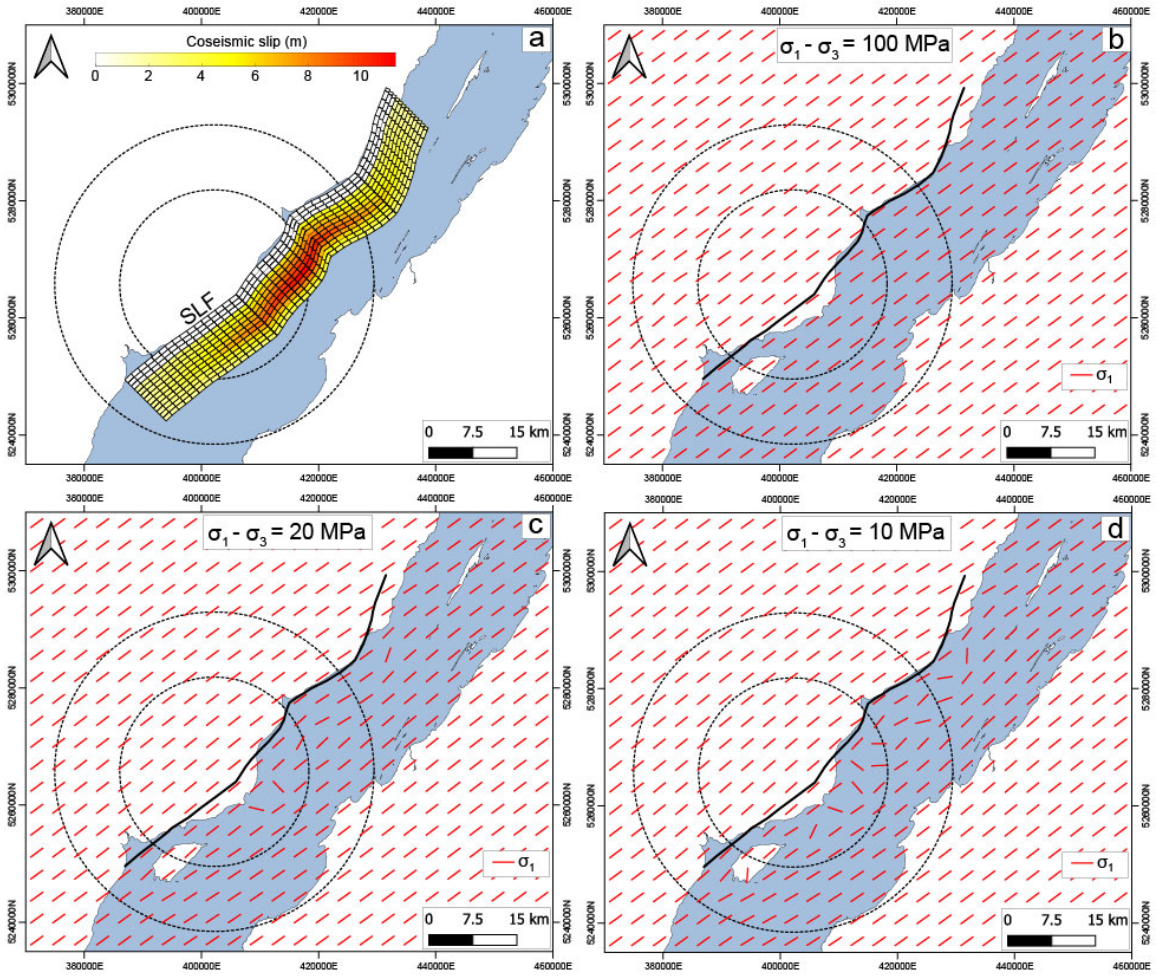

Figure S4. Modeled stress rotation due to coseismic slip of the 1663 Mw 7.5 Charlevoix earthquake calculated at 11 km depth. (a) Fault and slip model of the Saint Lawrence fault (SLF) used to calculate the stress rotation. Regional stress rotation calculated using (b) 100 MPa of background differential stress, (c) 20 MPa of background differential stress, and (d) 10 MPa of background differential stress. Dashed circles represent the Charlevoix meteorite impact structure.

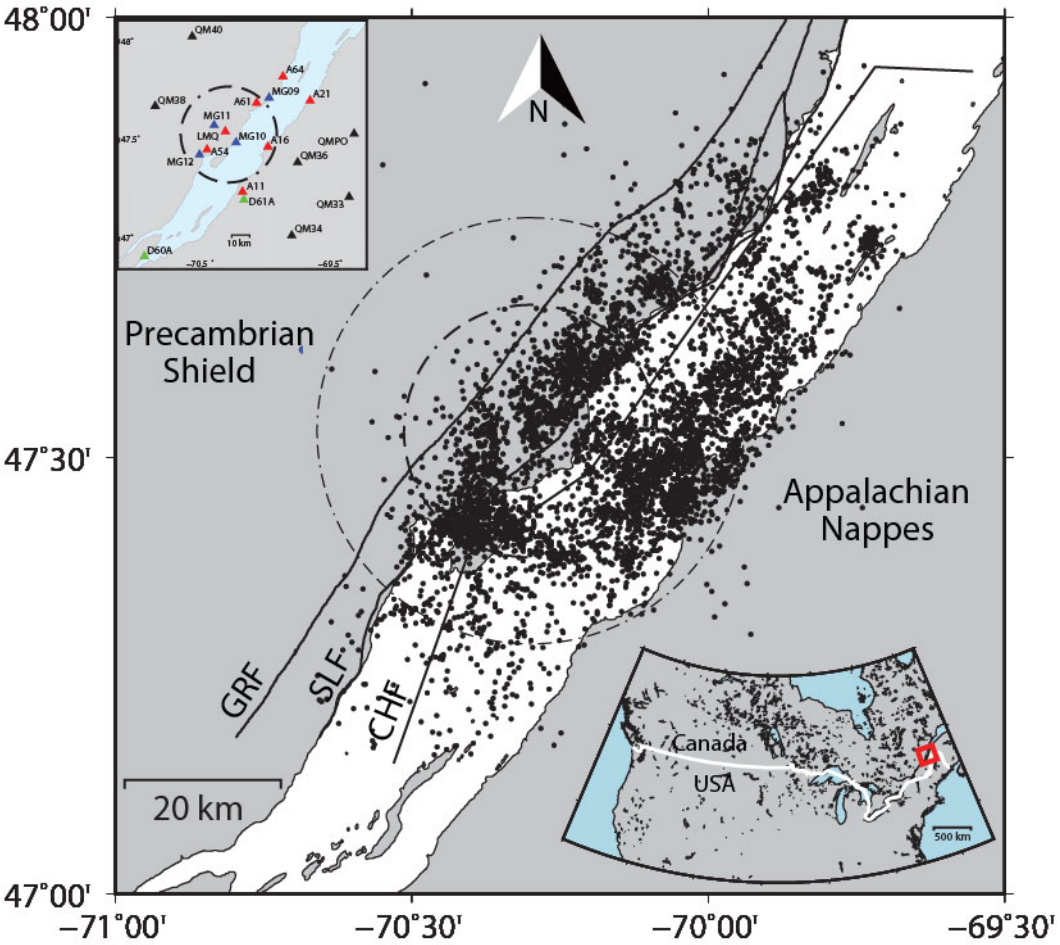

Figure S5. Distribution of 5663 earthquakes reported by Natural Resources Canada (NRCan) between January 1985 and May 2020. Dashed circle represent the Charlevoix meteorite impact structure. CHF, GRF, and SLF correspond to Charlevoix, Gouffre River, and St. Lawrence faults (Yu et al., 2016). Top-left inset: Broadband stations used in this study. Red, black, green and blue triangles represent CN, X8, TA and MG stations, respectively. Bottom-right inset: Red box represents the location of the study area.

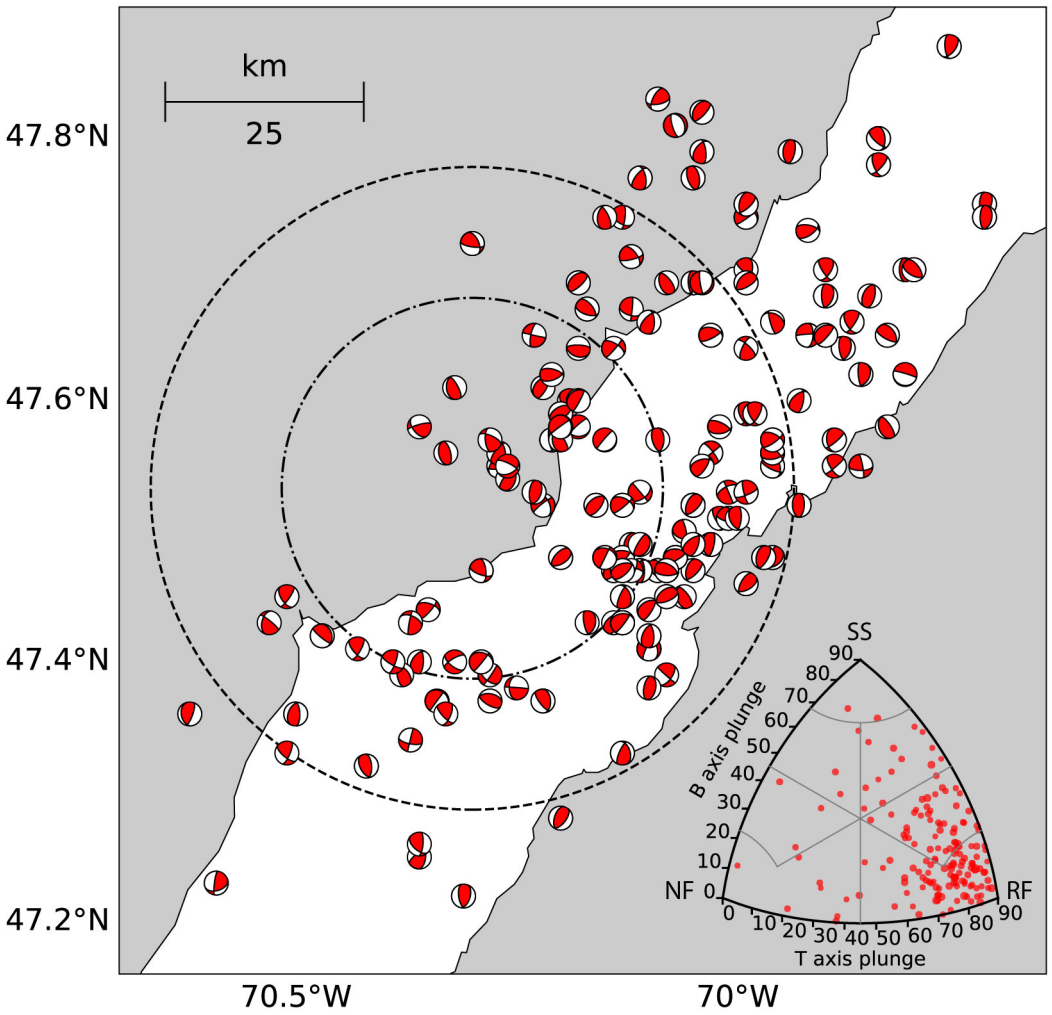

Figure S6. Focal mechanism (FM) solutions (161) computed with *Grond*. Bottom-right inset: Distribution of FM faulting style.

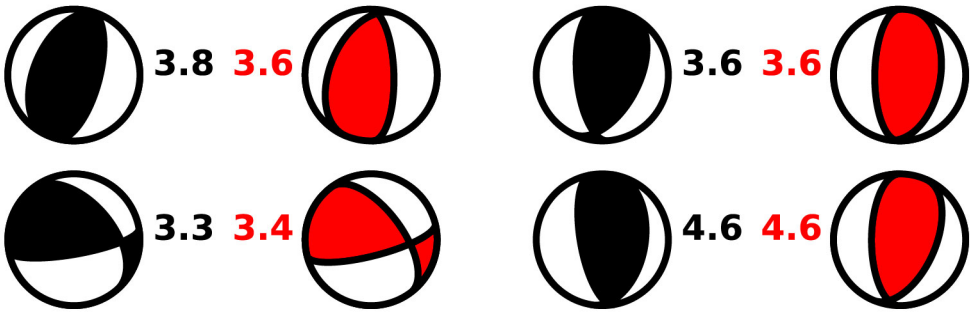

Figure S7. Comparison of FM solutions calculated here (red) and SLUEC catalog FMs (black) for 4 M 3+ events. The number beside each FM represent the moment magnitude estimated for the event.

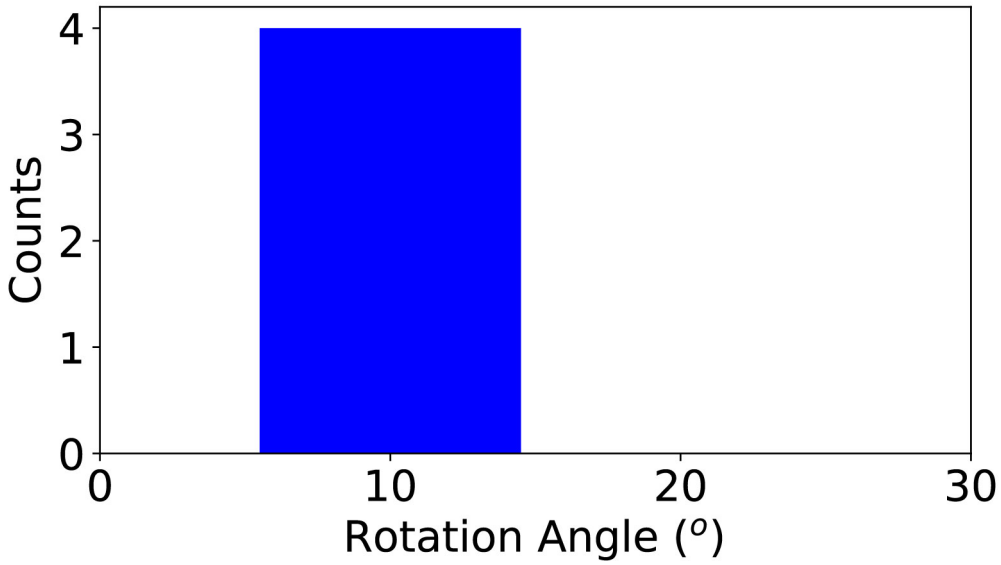

Figure S8. The Kagan angle of rotation between solutions calculated here and SLU catalog events shown in Figure S6.

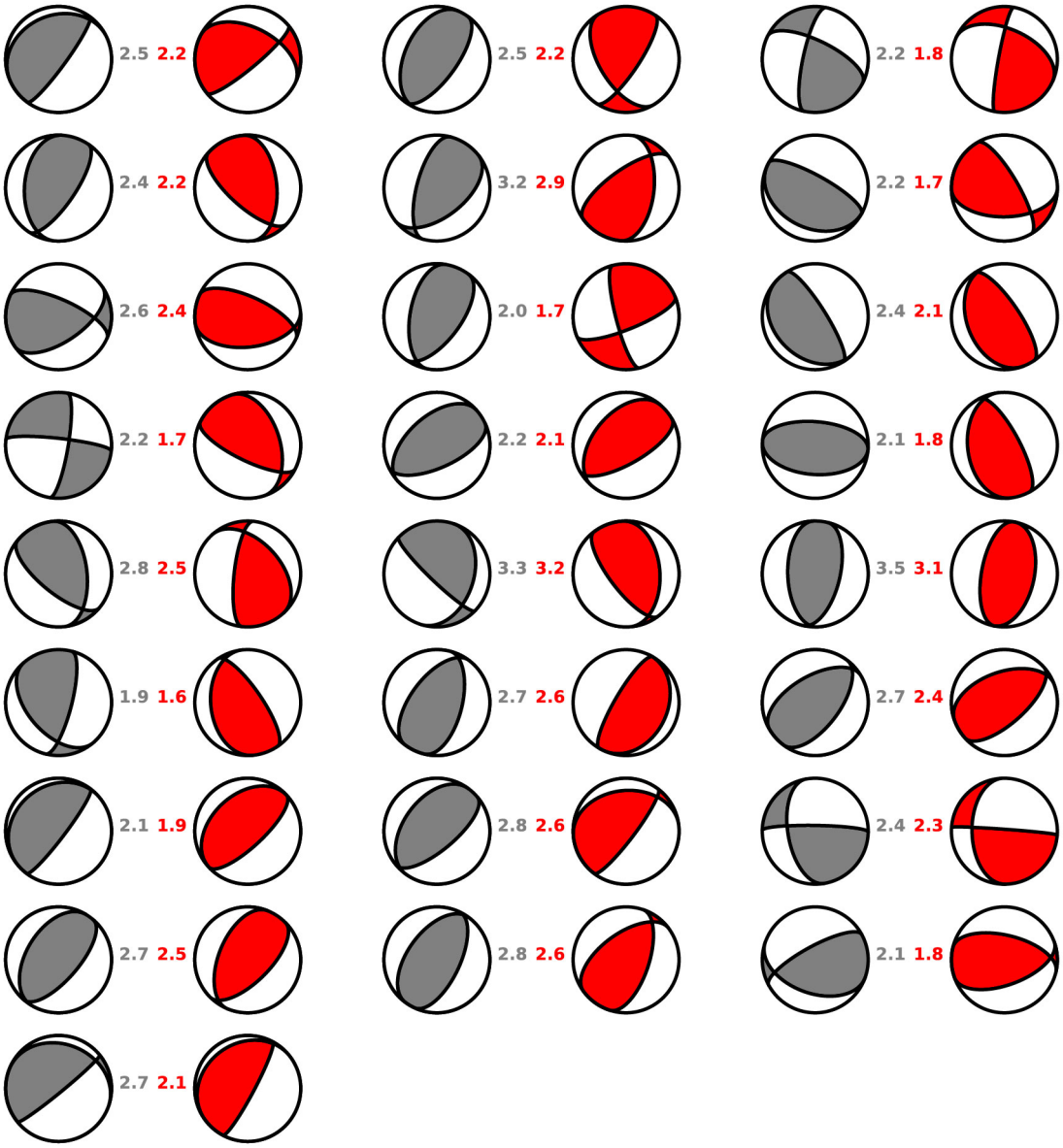

Figure S9. Comparison between 25 FM solutions determined with *Grond* (red) and *hybridMT* (gray). Estimated magnitude indicated next each FM in color corresponding to the method used.

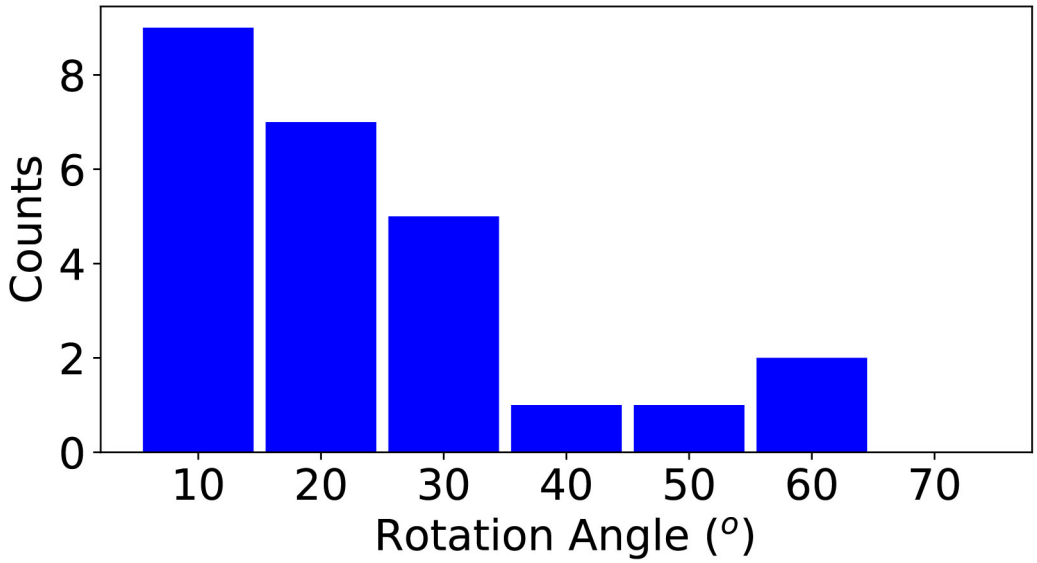

Figure S10. The Kagan angle of rotation between the two sets of solutions in Figure S8